DOI: 10.15480/882.9340

Eighth International Symposium on Marine Propulsors
smp'24, Berlin, Germany, March 2024

Propeller Design and Dynamic Hull-Propeller Interaction of an XLUUV

M. Kösterke*, J.-P. Voß, M. Riesner and M. Greve

thyssenkrupp Marine Systems, Kiel, Germany

ABSTRACT

The research work presented in this paper focuses on two topics. The first addresses a propeller optimization for a highly modular twin screw autonomous underwater vehicle, taking into account the propulsion efficiency and a low noise and vibration level. This includes the avoidance of cavitation in submerged and specified surfaced conditions and furthermore allows for a silent class notation. The second topic is a new approach to model ship-propeller interaction during fast acceleration maneuvers of the vehicle. This approach is deemed necessary for ships and submarines with high torque electric propulsion that can rapidly increase the rotation rate. In order to meet the high requirements for the propeller with an acceptable effort, a self-developed propeller series is used and a baseline propeller is optimized further. The simulation method for the prognosis of acceleration and deceleration performance uses a new unsteady formulation of wake fraction and thrust deduction as a function of the hull advance ratio within an analytical method. Main benefits of this method are a more realistic propeller operation point at high acceleration rates at maneuver start resulting in improved cavitation prediction. Maneuver predictions with the new approach are compared to CFD-simulations focusing on the wake fraction and thrust deduction during acceleration and deceleration of the vehicle.

Keywords

Propeller design, Propeller/hull/rudder interaction, Propulsor dynamics, Propulsion in off-design conditions, XLUUV

1 INTRODUCTION

In recent years large areas of the transport sector have undergone a transformation phase towards electrification. This also accounts for waterborne transport, where electric propulsion of ships potentially has major impact on system performance, mechanic design and hydrodynamics. Possible advantages are increased energy-efficiency reducing operational costs, emission reduction and noise reduction contributing to lower environmental impact and compliance with emission regulations and an enhanced maneuverability and safety due to a precise control of the system. Further advantages are reduced maintenance, scalability and the flexibility of combination with traditional propulsion. Corey & Moon (2021) give an overview on possible system layouts and operational implications for electrically driven naval vessels compared to conventional mechanical drives focusing on the system performance and cost effects. Challenges in the architecture design and control strategies of electrical and hybrid propulsion compared to mechanical propulsion is discussed by Geertsma et. al. (2017).

In addition to electrification, a second current trend is the extremely dynamic development of drone technology. Naval drones can be either swimming, ship-type drones or underwater drones. The latter vehicles are considerably smaller than manned submarines and usually propelled by small thrusters or propellers. Some of today's UUVs and AUVs are intended to operate independent of any surface mothership for a long time and require a significantly enhanced range. Having no energy connection to a surface ship through a tether, these vehicles have to be designed for energy efficiency. When operating in a sensitive natural environment, noise emissions are also required to be low. Therefore, the first part of the paper reports on the design and optimization of XLUUV-propellers for efficiency and noise using a self-developed propeller series in order to determine a good basic design.

When using an electric propulsion system on a vessel, its acceleration can be dynamic and a simulation of maneuvers including the cavitation onset is challenging. Due to the high torque at low speed, the hydrodynamic effects are different compared to mechanic propulsion and the use of the classic naval architecture propulsion coefficients is debatable. Following the usual definition, hull-propeller interaction is the difference between ship resistance test and propeller open-water test on one hand and self-propulsion test on the other hand. This definition results from the model-test driven assessment of ship propulsion beginning with the first model basin and the theory of Froude in the 19th century. The wake $(1-w)$ represents the change in propeller operating point due to the presence of the ship and the thrust deduction $(1-t)$ the change in pressure distribution on the hull due to the operating propeller. When investigating ship operation at different propeller loadings or unsteady maneuvers, the values of wake fraction and thrust deduction fraction vary. Several investigations have been undertaken in the mid 20th century and reported e.g. by Harvald (1967). Quite simple

formulas based on assumed velocities and propeller thrust loading have been implemented in performance prediction tools, see e.g. (Mizythras 2016). Full-scale measurements as e.g. reported by Artyszuk (2003) in order to investigate unsteady hull-propeller interaction often lack a good database due to measurement (or environmental) uncertainty. The situation with a submerged underwater vehicle is somewhat different, because wind and waves adding a large error margin to full-scale measurements can be avoided. Furthermore, the electric motor and its efficiency at various operation regimes is well-known and the drive-train layout is simple. This makes a quite exact assessment of the full-scale measurements feasible. With electric propulsion motors, very fast changes of propeller rotation rates are possible with only the inertia of the rotating parts and the added hydrodynamic mass as limiting factors.

When such maneuvers are evaluated, it is assumed to be insufficient to use a quasi-steady approach. The wake fraction and thrust deduction have to vary over time when using the classic propulsion equations. At the very beginning of a fast acceleration, the propeller operation point is near bollard-pull condition. Because the advance velocity of water to the propeller can be very low and at the same time the propeller suction effect is not distinct, the torque is mostly inertia-driven. After the first seconds, the shaft rotation rate is as large as allowed by the motor torque limit. The suction effect of the propeller is high resulting in low-pressure on the aft-ship and a high thrust deduction fraction. The value of wake fraction is, in the unsteady case, largely driven by the acceleration $\dot{u}$ and results from the known values of ship speed and propeller operation point. The present investigation makes use of the classical mathematical models for propulsion. Possibly, the traditional way of using wake fraction and thrust deduction does not cover all apparent effects, in particular when also using any kind of energy-saving device. Also, with new possibilities emerging from the constant growth of computational power, the total energy transformed by ship propulsion can be decomposed in new ways. Discussions are e.g. given by van Terwisga (2013) or Eslamdoost et al (2017). The present paper reports the determination of the unsteady trend of hull-propeller interaction from CFD-simulations and using the values for acceleration simulations.

2 The Test Case

Within the national research project MUM2 (Modifiable Underwater Mothership, grand 03SX439) thyssenkrupp Marine Systems develops a twin screw autonomous extra large unmanned underwater vehicle (XLUUV). Special attention during the actual MUM design process is paid to the overall efficiency of the propulsion and maneuvering system, because both the energy stored onboard and the available power of MUM are limited. Long-range missions with a distinct portion of submerged transit require low resistance, efficient main propulsion and dynamic stability. In contrast to that, the requirement for dynamic positioning leads to a demand for high actuator forces during slow or zero speed. These propulsion and maneuvering requirements result in a unique combination of propellers, rim-driven tunnel thrusters and azimuth thrusters. The multifunctional operation capabilities are realized with a highly modular design consisting of standardized 10'' modules and a hydrodynamic casing. The vehicle length can vary between 25m and 50m resulting in a total mass between 140t and 360t and reaching a maximum range of about 720nm at a design speed of 4kn (maximum speed of 8kn). A demonstrator vehicle of MUM in full-scale is currently under construction and is expected to begin sea-trials in 2025. This demonstrator is used as a reference case for the presented research work and Table 1 lists its main particulars.

Table 1: Main Particulars of MUM-Demonstrator

Speed	$[\boldsymbol{kn}]$	4
Length	$[m]$	26.0
Width	$[m]$	6.9
Height	$[m]$	3.5
Displacement	$[t]$	366

3 THEORETICAL BACKGROUND

3.1 Propeller Design

The propeller design is two-staged. At first, a propeller is chosen from a self-developed propeller series (Kösterke 2021). The series includes operational point cavitation optimized propellers. Because this series is based on numerical optimized propellers the cavitation inception is known in the early design stage, providing a quick solution for the optimal blade number and area ratio based on the real physical characteristics for the present propeller design. The detailed propeller design is performed based on a wake-adapted optimization applying a numerical method based on potential-theory. Objective functions are defined in order to optimize the predefined requirements and constrains by solving a minimization algorithm.

3.2 CFD

The main features of the applied CFD techniques are described in the following chapter. More details can be found in Ferziger and Peric (2002). The applied numerical method solves the Reynolds-averaged Navier-Stokes equations (RANSE) discretizing the fluid domain based on the finite volume approach. Each finite volume (cell) fulfils the conservation of mass, $m = \int_V \rho \, dV$, and momentum, $\vec{I} = m \cdot \vec{v}$. The fluid is assumed to be incompressible, isotherm and viscous, thus the conservation of mass follows from:

$$\frac{\partial}{\partial t}\int_V \rho \, dV + \int_S \rho \, (\vec{v} - \vec{v}_s) \cdot \vec{n} \, dS = 0 \qquad (1)$$

And the conservation of momentum from:

$$\frac{\partial}{\partial t}\int_V \rho\,\vec{v}\,dV + \int_S \rho\,\vec{v}\,(\vec{v}-\vec{v}_s)\cdot\vec{n}\,dS = \int_S T\cdot\vec{n}\,dS + \int_V \vec{b}\,dV \quad (2)$$

Here, $\vec{n}$ is the normal vector of each cell face, $\vec{v}$ is the fluid velocity, $\vec{v}_s$ the fluid velocity at each face, V the cell volume, S the face area and ρ the fluid density. The surface and volume forces are included in the stress tensor, T, and in the body force vector $\vec{b}$. T includes viscous shear stresses based on the dynamic viscosity, μ, and pressure terms, p, and follows from

$$T = \mu\{\nabla\vec{v} + \nabla\vec{v}^T\} - p\boldsymbol{I} \quad (3)$$

The index T designates the transpose of the vector and $\boldsymbol{I}$ is the unit tensor.

An implicit second order scheme is applied for time integration and a Semi-Implicit Method for Pressure-Linked Equations (SIMPLE) algorithm (Ferziger and Peric, 2002) ensures an implicit coupling between pressure and velocity. The k-ω-SST turbulence model and a wall function are applied for turbulence modeling.

RANSE-simulations using ANSYS-CFX were carried out for the stationary and accelerated XLUUV in both towed and self-propelled condition with the aim of accurately predicting the propeller-hull interaction and providing a database for the analysis of the unsteady thrust deduction and wake fraction and their acceleration dependency.

A stationary resistance simulation was initially performed to predict the hull resistance and determine the required propeller thrust at self-propulsion for an estimated thrust deduction factor. The thrust was verified afterwards by a stationary propulsion simulation. The propeller thrust was modeled by a body-force model based on axial momentum sources. The data obtained from these two simulations, i.e. resistance, thrust, nominal and effective wake, are the basis for the initial propeller design.

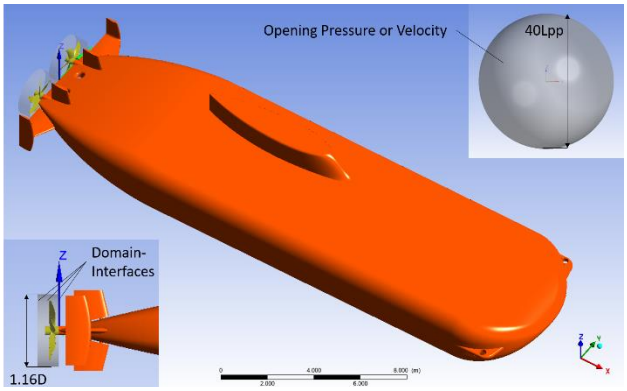

Figure 1; CFD-Model for the stationary and accelerated propulsion-test

After completion of the propeller design process (see 4.1) the final design was verified in a stationary propulsion-test with geometrically discretized propellers. The propeller shaft speed was iteratively adjusted until attaining thrust-resistance equilibrium. The advance coefficient at self-propulsion point was evaluated via thrust-identity based on the calculated (RANSE) propeller open-water diagram.

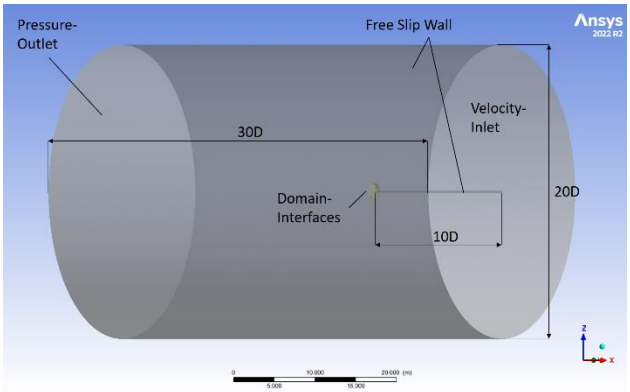

Figure 2: CFD-Model for the propeller open-water tests

Two additional propulsion-tests with a self-propelled (free in surge) model were performed in order to determine the unsteady propulsive quantities. A time-dependent equation prescribed the propeller shaft-speed. To investigate two different vehicle accelerations, the vehicle mass was decreased to 10% of the fully submerged displacement during the second numerical computation. For the quantification of the hydrodynamic added mass of the submarine, the first case with mass equivalent to 100% of the displacement was repeated without propellers but driven by a constant external force. The extraction of the hydrodynamic mass from the results is shown in chapter 3.3.

All stated simulations were performed at full scale in order to consider the correct boundary layer thickness and avoid any scale effects. Since the unsteady propeller-hull interaction is of particular interest in this study and strong pressure/thrust-fluctuations could already be observed during the stationary propulsion-test (when the propeller blades passing the transom at 3 and 9 o'clock position), it was decided to perform all following propulsion-tests with geometrical discretized propellers. So neither tangential- and/or radial averaging nor a body-force model is applied in the simulations.

The computational model of the propulsion-tests shown in Figure 1 consists of a spherical background domain and two propeller domains for the starboard side and portside propeller. The propeller domains are connected to the background domain via non-matching (sliding) domain-interfaces. At the outer boundary of the background domain a Dirichlet boundary condition for the velocity field was applied and a pressure reference location was set for the stationary case. An "Opening Pressure" boundary condition – prescribing a relative pressure level and permitting mass flux into and out of the domain – was used for the self-propelled case. In the latter case, a flow-field coupled motion solver calculated the acceleration of the XLUUV. Therefore, a rigid body was defined containing the hull and propellers.

The computation model and boundary conditions for the propeller open-water tests are shown in Figure 2. A

cylindrical, non-rotating background domain was created and the propeller-domain/mesh from the portside propeller of the propulsion-tests connected via non-matching (sliding) domain-interfaces.

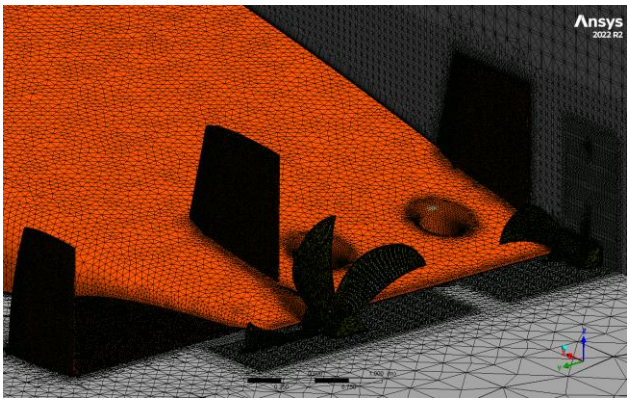

Figure 3: Mesh resolution at aft ship and propellers

Surface- and volume-grid refinements were placed at the aftship, rudders and propellers in order to sufficiently resolve the wake of the casing on the topside of the hull and the interaction of the propellers with the rudders and the hull, see Figure 3. The volume-mesh of the background domain consists of 8.08 million nodes and of the propeller domains 3.6 million nodes each.

3.3 Acceleration Model

The unsteady formulation is introduced to capture the effects of a strongly increasing propeller rotation rate due to the electric propulsion. The acceleration rate is only limited by the inertia of the rotating parts and the added hydrodynamic mass. With a greatly varying propeller loading during fast acceleration and deceleration, the classic quasi-stationary approach for ship-propeller interaction is extended to enhance accuracy.

The corresponding investigation focusses on the interaction between ship and propeller during fast acceleration maneuvers. Therefore, possibilities of determining and modeling the interaction using different approaches are discussed in this chapter. A description of wake fraction and thrust deduction fraction for stationary condition is e.g. given by (Kerwin 2010). For a ship in self-propulsion condition the general formulation of forces in forward direction for unsteady condition reads as follows:

$$T \cdot (1-t) = R_T(u) + (m+X) \cdot a \qquad (4)$$

Here the left hand side of the equation inherits the forces caused by the propeller. The right hand side contains the resistance and the inertia forces including body forces. When multiplying T with the thrust deduction $(1-t)$ the useful thrust results, which - for a steady ship speed - equals the (stationary) ship resistance R_T.

The next passages describe the analytical acceleration method followed by a description of different methods for determining the hull-propeller-interaction from the numerical simulations.

Analytical Acceleration Method

A simple and fast method based on the 1978 ITTC performance prediction method (ITTC 2011) is used to predict the acceleration of a submarine. The critical issue for computing realistic results is to use exact input data for the simulations. These are e.g. engine characteristics, system inertia, propeller characteristics and system control. The present model consists of a velocity-stepping method which uses the max. torque $[Q_{\max}(n)]$ characteristics of the electric motor as a boundary condition. Here the self-propulsion state is determined for a discretized array of velocity steps,

Since torque and thrust of a propeller in behind condition are considered to be linked to the open water characteristics via the relative rotative efficiency η_R, an equilibrium for the maximum torque can be found for each time step.

As the thrust and torque coefficient characteristics $[K_T(J)$ and $10K_{QO}(J)]$ are known, the following equation system containing the unknowns of the rotation rate n and the time step Δt can be computed.

$$10K_{QB} = \frac{10 \cdot Q_{\max}(n)}{\rho n^2 D^5} = 10K_{QO}(J) \cdot \frac{1}{\eta_R} \qquad (5)$$

$$K_T(J) = \frac{R_T(u)+(m+X)\cdot a}{(1-t)} \cdot \frac{1}{\rho n^2 D^4} \qquad (6)$$

Containing:

$$\Delta t = \frac{\Delta u}{a} \qquad (7)$$

$$J = \frac{u \cdot (1-w)}{n \cdot D} \qquad (8)$$

Here the wake fraction w, the thrust deduction fraction t and the relative rotative efficiency η_R are not constant but depend on the actual condition of ship and propeller. Thrust and torque can be calculated from the propeller open water data for the actual advance ratio J. The thrust available for accelerating the submarine T_{acc} can be determined similar to the torque from the right-hand side of equation (4).

The acceleration a can then be calculated according to equation (4). It is obvious that the values of, t and η_R largely influence the whole maneuver. During an acceleration maneuver both sides of equation (4) increase significantly due to inertia and the increasing thrust. The trend of thrust deduction wake fraction and relative rotative efficiency are given depending on the hull advance ratio J_H, reflecting the difference of actual speed u and the time dependent revolution rate n and can be regarded as rate of acceleration.

3.4 System Identification based on Numerical Simulations

In order to break down the interaction between vessel and propeller, a set of numerical simulations is mandatory to isolate necessary information. Analogues to classical model tests these numerical simulations are described as follows:

Simulation cases for steady state conditions:

I. Ship resistance

II. Self-propulsion

Additional simulation to determine the propulsion coefficients for steady state or transient conditions:

III. Propeller open water characteristics

Simulation cases for transient conditions:

IV. Acceleration without propeller

V. Acceleration with propeller

From case IV and I the resistance R_T and the hydrodynamic added mass X can be determined.

$$F_x \text{ IV} = R_T(u) + Xa \tag{9}$$

Case V gives the thrust T and the acceleration $\dot{u}$ during the maneuver. Combining case V and VI, equation (4) can be derived to compute the thrust deduction:

$$t = \frac{T - (R_T(u) + (m + X) \cdot a)}{T} \tag{10}$$

The propeller open water simulation case III together with the accelerated self-propulsion case V were used to determine the wake fraction coefficient w and relative rotative efficiency η_R. Under the assumption of thrust identity:

$$K_{TO}(J) = K_{TB} \tag{11}$$

The interaction coefficients follow from:

$$w = 1 - \frac{J \cdot n \cdot D}{u} \tag{12}$$

$$\eta_R = \frac{10K_{QO}(J)}{10K_{QB}} \tag{13}$$

The values of the interaction coefficients determined by the results of the numerical simulations are discussed in the following chapters.

4 RESULTS

The outcome of the present research consists of propeller design, numerical results, ship propeller interaction and resulting acceleration model and is presented and discussed below.

4.1 Propeller Design

The propeller design is based on a series of design point optimized propellers. By taking cavitation into account during the regression, the optimal blade area ratio of the propeller can be determined based on the required cavitation number for a given thrust loading coefficient. Determining the cavitating tip vortex diameter by using the Hamel-Oseen Vortex adds further knowledge about cavitation properties of the propeller design (Kösterke, 2021).

4.1.1 Design Procedure

1. Based on the regression a 5-bladed small area ratio propeller is chosen.

2. Starting with these parameters, a detailed wake adopted propeller design is carried out. The propellers are designed for a full-scale self-propulsion wake field obtained by CFD calculations using a body force model.

3. In order to minimize the noise radiation of the propeller an optimality criteria is defined to achieve a minimum pressure and force fluctuation level as well as avoidance of cavitation in the defined operation points.

4. The propeller calculation is carried out using an in-house potential flow lifting surface method.

5. The weighting between the different constraints is adjusted in order to achieve the best compromise for the vessel.

4.1.2 Design Result

The main dimensions of the propeller resulting from the optimization are listed in Table 2.

Table 2: Propeller Main Dimensions

Direction			**Outwards**
No. Blades	Z	$[-]$	5
Diameter	d	$[m]$	1.800
Area Ratio	A_E/A_O	$[-]$	0.389
Mean Pitch ratio	P_{mean}/D	$[-]$	1.014
Pitch Ratio R=0.7	$P_{0.7}/D$	$[-]$	1.220
Skew	θ	$[°]$	24.516

Figure 4 shows the final propeller geometry with the characteristic small blade area ratio distributed on five blades and sufficient skew to keep force and pressure fluctuations low.

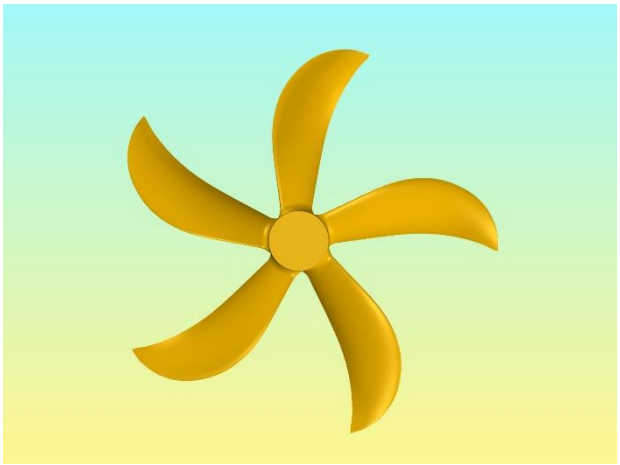

Figure 4: Propeller Design

According to the results, the operational thrust range for 8 kn does not lead to a local pressure level below vapor pressure (including the pressure level in the tip vortex). Thus, no cavitation is expected during normal operation.

4.2 Numerical Simulation Results

The results of the CFD simulations discussed in this chapter refer to a quasi-steady state self-propulsion simulation and fully unsteady acceleration simulations.

4.2.1 Results of Quasi-Steady Simulations

To determine the interaction behavior caused by the unsteadiness of the acceleration process, the stationary quasi self-propulsion state is investigated first. In this case, constant forward speed is reached by finding the equilibrium of longitudinal forces. For 4 kn the following self-propulsion conditions are identified:

Table 3: Self-Propulsion Point

Speed	v_S	$[kn]$	4
Relative rotative efficiency	η_R	$[-]$	1.016
Open water efficiency	η_o	$[-]$	0.691
Advance ratio	J	$[-]$	0.817
Thrust coefficient	K_T	$[-]$	0.201
Torque coefficient	$10K_Q$	$[-]$	0.376
Thrust loading	C_{TH}	$[-]$	0.846
Thrust deduction	t	$[-]$	0.167
Wake fraction	w	$[-]$	0.298

For assessing the ship-propeller interaction in detail, the pressure distribution on the hull and the velocity distribution in different planes in the aft ship region are examined more closely.

In order to display the velocity field the propeller operates in, the local velocity in a plane a short distance upstream of the propeller is evaluated. The local propeller characteristics in which the propeller operates during one revolution can be identified by visualizing the local advance coefficient J_{local} defined as the ratio of the local velocity and $n \cdot D$.

As illustrated in Figure 6, due to the propellers being arranged very close to the hull, the vessel has very pronounced low velocity zones behind the hull and almost undisturbed zones in the upper and lower area of the wake field. For this state, the effect of the single propeller blades influencing the local flow seems to be superimposed by the general flow velocity, which can be explained by the small thrust loading.

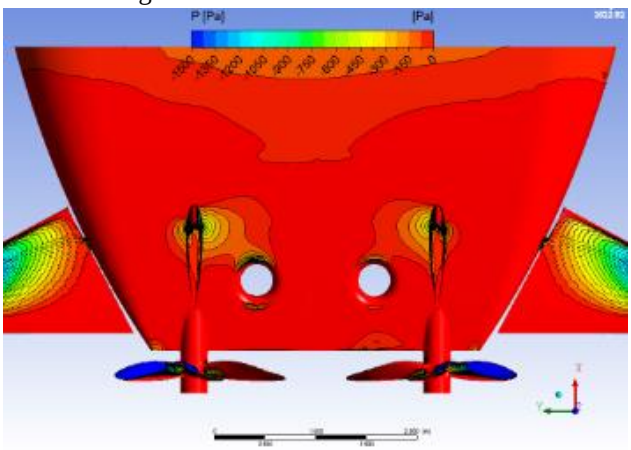

Figure 5: Pressure-Distribution at stern for the stationary propulsion test at $u = 2.0 m/s$

Figure 5 shows the pressure distribution at the aft ship. It can be seen that the local influence of the propeller on the hull is small.

4.2.2 Results of Unsteady Simulations

To understand the interaction behavior between ship and propeller during the acceleration maneuver, the wake and pressure characteristics are discussed during an early acceleration state and an advanced acceleration state.

Early state of the acceleration process.

A low speed of the vessel and high acceleration rate characterize the early state of the acceleration maneuver.

This leads to a dominance of the propeller effects on the velocity field between ship and propeller.

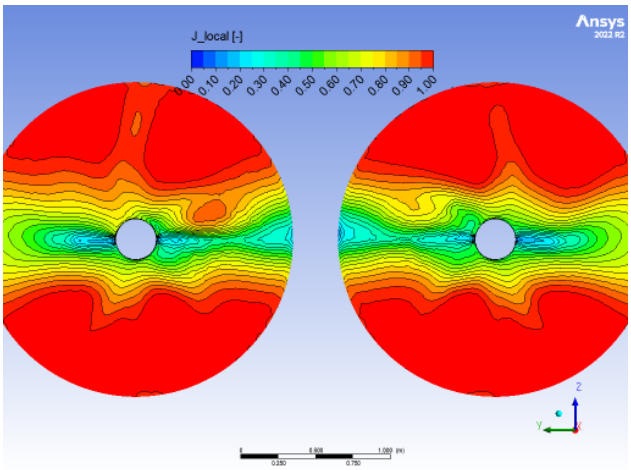

Figure 6: Local advance coefficient in a vertical plane 0.16D upstream of the propeller for the stationary propulsion test at $u = 2.0\ m/s$

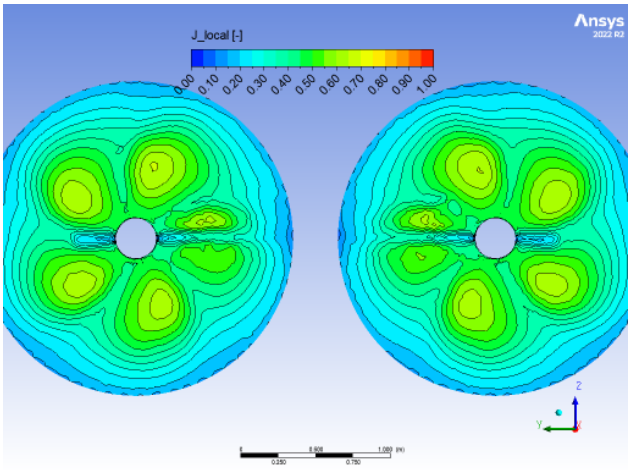

Figure 7: Local advance coefficient in a vertical plane 0.16D upstream of the propeller for the accelerated propulsion test at $u = 0.3\ m/s$ and $a = 0.03 m/s^2$

The supremacy of the propeller effects is illustrated in Figure 7, which represents the early state of the acceleration maneuver with a vessel speed of 0.3 m/s. During this state, a high wake fraction emerges due to a slow average inflow velocity and a high propeller induced angular velocity. During the high acceleration maneuver at low forward speed, the local velocity field is mainly induced by the rotating propeller, the hull contributes only marginally.

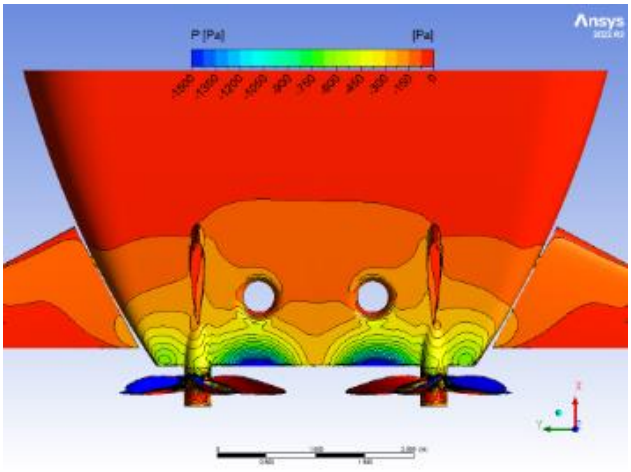

Figure 9: Pressure-Distribution at stern for the accelerated propulsion test at $u = 0.3\ m/s$ and $a = 0.03\ m/s^2$

The surface pressure distribution on the aft ship for this state is shown in **Figure** 9 and indicates high pressure disturbances close to the propellers, but less influence on the more forward parts. With this consideration the low thrust deduction is justified even if the local pressure close to the propeller could mislead to the assumption that the propeller pressure influence on the hull is higher than in the steady state.

Advanced state of the acceleration process.

During this state, the forward speed is significantly larger, but the acceleration rate smaller than in the previous state:

In Figure 8 the transition between the dominance of propeller caused effects and hull caused effects on the wake field is illustrated. Here the mean advance coefficient is getting closer to the stationary value but local effects of the single propeller blades are still visible.

Figure 10 confirms that this is at a transitory phase between high acceleration and quasi-steady state. The local propeller pressure effects are still present but the general pressure field along the hull has also decreased leading to an increase in thrust deduction.

4.3 Ship-Propeller Interaction

In order to display the unsteady hydrodynamic propulsion behavior, the commonly used propulsion coefficients according to equations 9, 11 and 12 are computed for the whole acceleration maneuver. In order to identify the difference between the effects caused by the different inflow velocities and leading to different advance coefficients and the actual change in velocity, two geometrically identical versions of the XLUUV were

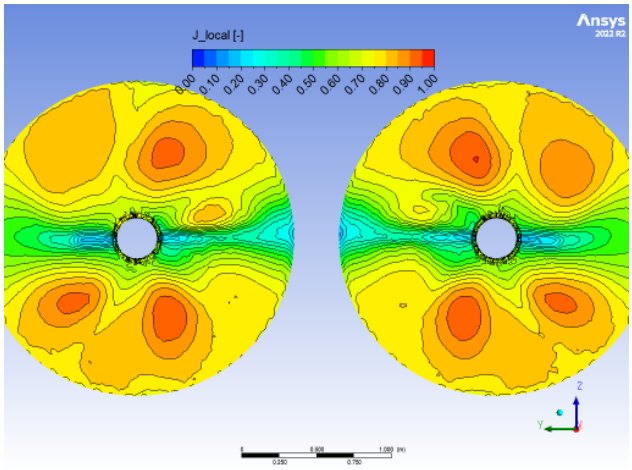

Figure 8: Local advance coefficient in a vertical plane 0.16D upstream of the propeller for the accelerated propulsion test at $u = 2.0\ m/s$ and $a = 0.015\ m/s^2$

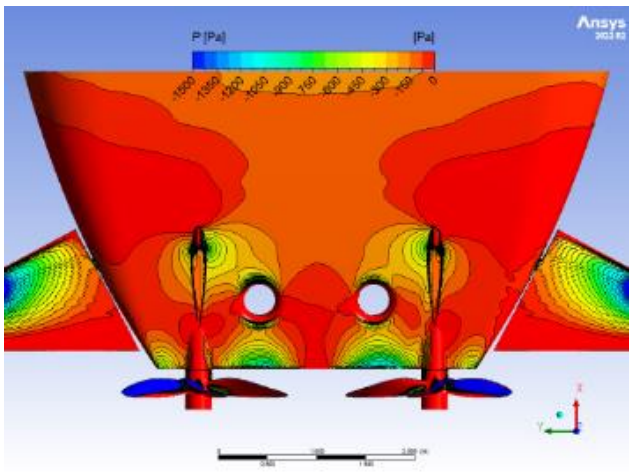

Figure 10: Pressure-Distribution at stern for the accelerated propulsion test at $u = 2.0 m/s$ and $a = 0.015 m/s^2$

investigated: One having the actual mass of 366t and one with 10% of the actual mass, leading to two simulations were the whole advance coefficient range is covered at different acceleration rates. Since the propeller advance coefficient depends on the wake fraction (see Eq. 8), all propulsion coefficients are displayed relative to the hull advance coefficient J_H which is computed using the ship velocity u instead of the inflow velocity.

4.3.1 Thrust deduction

The behavior of the thrust deduction during the acceleration process is computed by eq. 6 using the stationary resistance characteristics and the actual thrust computed during the numerical simulation. The hydrodynamic added mass X is determined by two additional numerical simulations in which accelerated resistance tests were performed applying two different acceleration rates. Figure 11 displays the development of the thrust deduction coefficients during the acceleration maneuver for the 366 t and the 36.6 t case.

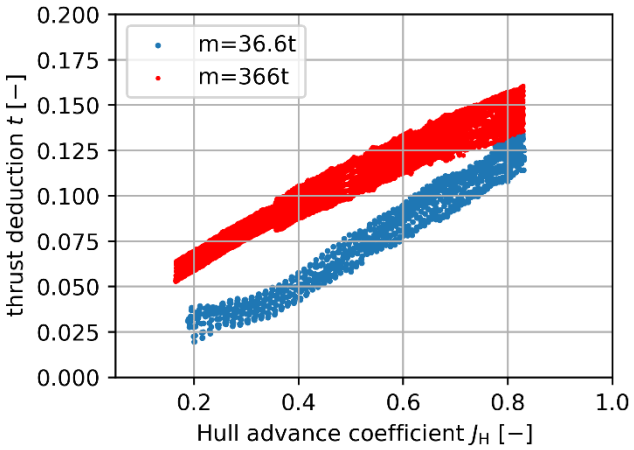

Figure 11: Variation of the thrust deduction coefficient over the hull advance coefficient.

From the results shown in Figure 11 it becomes evident that the thrust deduction factor increases during acceleration and towards the steady-state value. Its gradient depends on the forward speed and the acceleration.

4.3.2 Wake fraction

For the acceleration investigation the wake fraction is determined by using the thrust identity as described by Eq. 7 and Eq. 8.

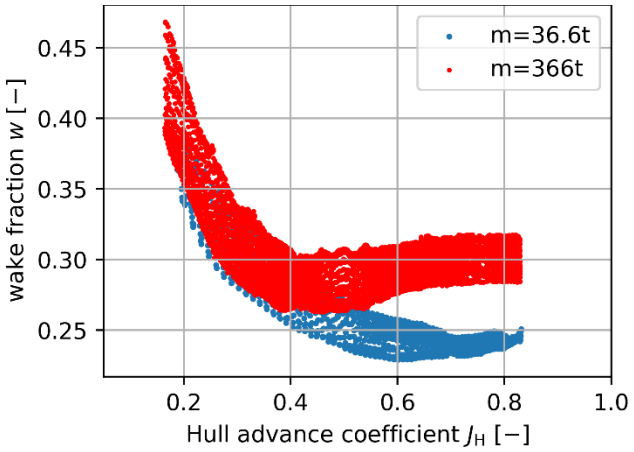

Figure 12: Variation the wake fraction coefficient over the hull advance coefficient.

Figure 12 depicts the trend of the wake fraction during acceleration. It can be seen that the influence of the vessel's actual speed appears to be dominant during the first half of the acceleration, while in the second half, the impact of the acceleration itself becomes more pronounced. During the slower accelerating maneuver with 366t of vehicle mass, the steady state wake fraction of w = 0.298 was reached earlier and overshoots less, compared to the faster accelerating case with 36.6t vehicle mass.

4.3.3 Relative rotative efficiency

When applying thrust identity, the relative rotative efficiency needs to be taken into account to factor in the effects of the inhomogeneity of the vessels wake field on the torque needed to generate the required thrust.

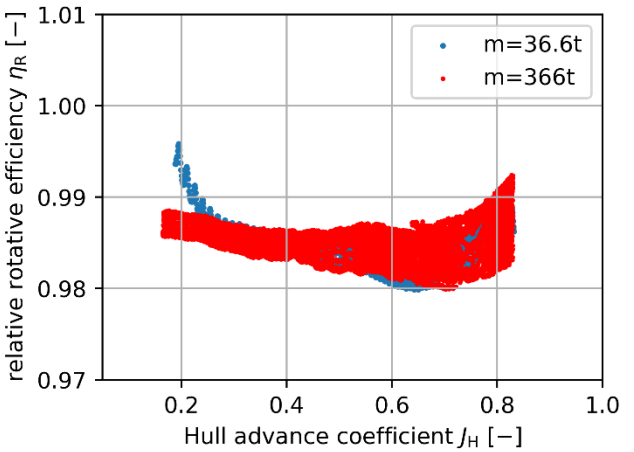

Figure 13: Variation of the relative rotative efficiency over the hull advance coefficient.

As illustrated in Figure 13, the propulsion efficiency factor appears to remain nearly constant regardless of the rate of acceleration. It only begins to reach the steady-state magnitude in the advanced stages of acceleration.

4.4 Acceleration Simulation

The acceleration model that is applied to investigate the influence of the unsteady ship propeller interaction during the general acceleration maneuver was already discussed in section 3.3. By performing one simulation using the constant self-propulsion coefficients and one simulation using the interaction characteristics determined in section 4.3, the effect of the unsteadiness can be evaluated. Therefore, the descriptive indications of the acceleration process are examined in more detail and compared to the CFD results.

Acceleration Rate

The first characteristic parameter is the acceleration rate a, which describes the change of speed during the acceleration process.

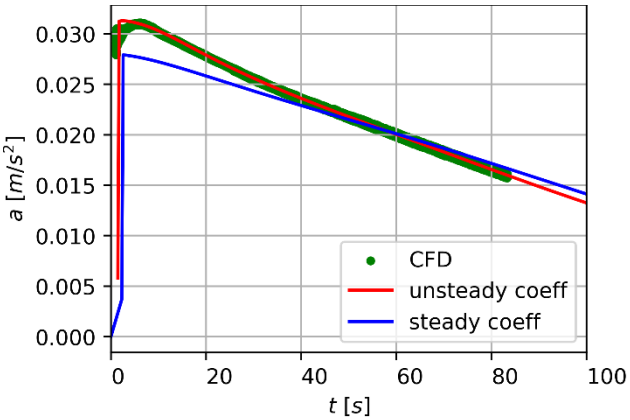

Figure 14: Acceleration rate for simulations using steady and unsteady propulsion coefficients and CFD results.

As displayed in Figure 14, the utilization of steady coefficients initially results in a lower rate of acceleration and, in the advanced stages, a slightly higher rate of

acceleration. In contrast, the employment of unsteady coefficients closely aligns with the CFD results.

Speed

The second characteristic parameter for the acceleration maneuver is the vessel's speed over the time which is shown by the graphs of Figure 15.

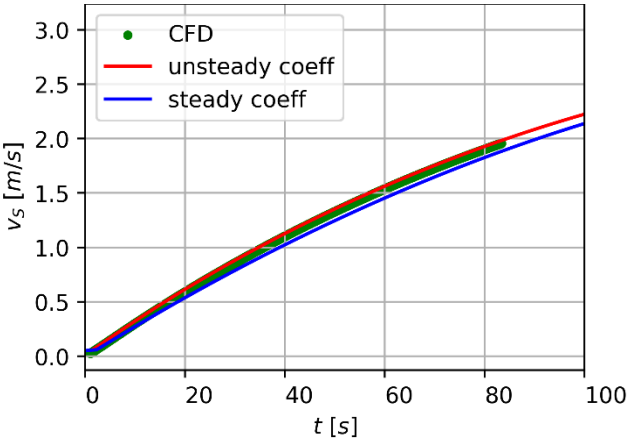

Figure 15: Speed over time for simulations using stationary and unsteady propulsion coefficients and CFD results

The behavior of the speed is analogous to the acceleration, indicating a slight underestimation of the speed while using steady coefficients. Whereas the usage of unsteady coefficients is matching the CFD results well. However, the graphic also shows that the influence on the speed is relatively low.

Distance traveled

Particularly for this type of autonomuos vessel the distance travelled during the acceleration maneuver is of special interest to correctly predict the position during the maneuver.

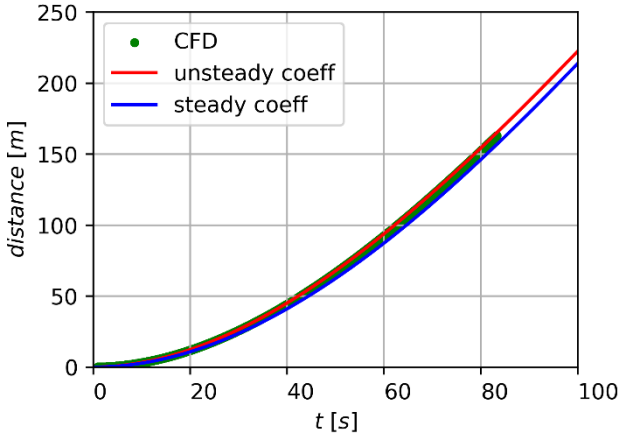

Figure 16: Distance traveled over time for simulations using stationary and unsteady propulsion coefficients in comparison CFD results

Even though the influence of the unsteady interaction on acceleration and velocity is clearly visible, Figure 16 shows that the influence on the traveled distance is almost negligible, which can be explained by the fact that the differences in the approaches are very small compared to the absolute value of velocity and acceleration.

5 CONCLUSIONS

In summary, within the scope of this study, a propeller for an XLUUV has been successfully designed to meet all specified requirements. To assess dynamic interactions, an analytical simulation model for acceleration maneuvers was developed, taking into account the interaction between the vessel and the propeller. Furthermore, to determine unsteady interaction effects, comprehensive transient CFD acceleration simulations with geometrically discretized propellers were conducted. From the results of these simulations, speed- and acceleration-dependent interaction coefficients were derived.

A comparison between the use of steady and unsteady interaction coefficients in the analytical acceleration simulation reveals that while the use of unsteady coefficients can enhance the results, the influence on the key parameters remains relatively modest.

For future work, a more detailed investigation of cavitation inception during acceleration in relation to the unsteady wake field could be of interest.

Since a demonstrator of the XLUUV is under construction at the moment it is likely that some of the results gained by this research could be verified by full-scale measurements.

Acknowledgement

The research was founded by the Federal Ministry for Economic Affairs and Climate Action under the grand 03SX543A.

REFERENCES

Artyszuk, (2003), A novel method of ship manoeuvring model identification from sea trials, Annual of Navigation, no. 6,

Corey, C. & Moon, H. (2021). 'Electric Propulsion for Modern Naval Vessels', Proceedings of International Maritime Defence Industry Exhibition MADEX 2021, Busan, South Korea

Eslamdoost, A., Andersson, J., Bensow, R., Gustafsson, R. & Hyensjö, M. (2017). 'Analysis of Propeller-Hull Interaction Phenomena on a Self-Propelled Axisymmetric Body', Proceedings of the Fifth International Symposium on Marine Propulsors smp'17, Espoo, Finland

Ferziger, J., Peric, M., (2002). Computational Methods for Fluid Dynamics 3rd ed., Springer Berlin, Berlin Heidelberg New York.

Geertsma, R.D., Negenborn, R.R., Visser K. & Hopman, J.J. (2017). 'Design and control of hybrid power and propulsion systems for smart ships: A review of developments', Applied Energy 194, 30–54

Greve, M., Rentzow, E., Kurowski, M., Ritz, S., Golz, M., Bayazit, N. & Vijayasarathi, L.N. (2022). 'Design

of the Propulsion System for the autonomous XLUUV MUM', Proceedings of the ASME 2022 41st International Conference on Ocean, Offshore and Arctic Engineering OMAE2022, Hamburg, Germany

Harvald, SV. AA. (1967). 'Wake and Thrust Deduction at Extreme Propeller Loadings', Publications of the Swedish State Shipbuilding Experimental Tank, Nr. 61

Kalwa, J., Stach, R., Bannasch, R., Olenew, E., Wehner, W.-H., Richter, N., Golz, M., Ritz, S., Holbach, G., Kurowski, M., Rentzow, E. & Jeinsch, T. (2021). ‚MUM - Erarbeitung einer meerestechnischen Systemlösung für autonome Unterwasser-Arbeiten', Statustagung Maritime Technologien, Forschungszentrum Jülich, pp. 67-75, (in german)

Kerwin, J. E. & Hadler, J. B. (2010). ‚The Principles of Naval Architecture Series: Propulsion', The Society of Naval Architects and Marine Engineers, Jersey City, New Jersey, 978-0-939773-83-1.

Kösterke, M (2021). 'Entwicklung eines polynombasierten Propellerentwurfsverfahrens mit Berücksichtigung der Kavitation' , Master Thesis, Institut für Land- und Seeverkehr, Fachgebiet Dynamik Maritimer Systeme, Technische Unversität Berlin, Germany, (in german)

Mizythras, P., Boulougouris, E. & Theotokatos G. (2016). 'Computational investigation of ship propulsion performance in rough seas', Proceedings of the International Conference on Maritime Safety and Operations, Glasgow, UK

Terwisga, T. (2013). 'On the working principles of Energy Saving Devices', Proceedings of the Third International Symposium on Marine Propulsors smp'13, Launceston

'1978 ITTC Performance Prediction Method', ITTC - Recommended Procedures and Guidelines, (2011)